

COMPUTATIONAL ANALYSIS ON THE EFFECTS OF LEADING EDGE TUBERCLES ON THE PERFORMANCE OF ROTATING PROPELLER

D. Di Pasquale¹, Ta. Tarun², S. Shubham¹, S.A. Prince¹ & A. Proenca¹

¹School of Aerospace, Transport Manufacturing, Cranfield University,UK ²Indian Institute of Technology(BHU),Varanasi, India

Abstract

This research paper focuses on investigating the effect of leading edge tubercles on the performance of rotating propellers. The primary objective of this study is to assess if biologically inspired passive flow control techniques, particularly tubercles, seen on whale fins, could be employed to suppress flow separation on rotating propeller blades. Such an effect could improve the thrust and power performance of propellers. The study involved the assessment of various leading edge tubercles of various sizes and extent on a three blade propeller. Computational analysis, encompassing RANS, unsteady viscous vortex panel method, and Lattice Boltzmann Method (LBM) solvers showed that these tubercles can have a positive effect in terms of thrust generated at a particular RPM. These results are validated against experimental acquired from a wind tunnel test of the propeller. The experimental results also showed, that for a given rotational speed up to an RPM of 3000, tubercles which cover the full span of the blades increased the thrust generated. This effect increased with increasing RPM, a trend also captured in the CFD analysis.

Keywords: Rotating propeller, Aerodynamic performance, Leading-edge tubercles, Stall delay, Numerical simulations

1. Introduction

Nature has been a significant inspiration to mankind for thousand of years, particularly in the engineering field. The term 'Biomimicry' coined by Janine Benyus, explains the concept as nature having already optimised biological performance over millions of years and through the process of natural selection. The application of biologically inspired engineering mechanisms has created highly efficient solutions to resource efficiency and management problems that humans have faced in recent years. The tubercles found on the flippers of the Humpback whales have shown unique characteristics of reducing or delaying the flow separation on the flippers allowing these marine mammals to better manoeuvre their large bodies with ease. Many researchers, for instance [1, 2, 3] have found that when the tubercles have been applied to the leading edge of a wing, they help delay flow separation at high angle of attack and thus improving the lift to drag ratio. However very little research have been done on the effect tubercles have on a rotating blade. Tubercles are expected to act in a comparable way to vortex generators, forming boundary layer embedded vortices to enhance mixing, but there is no experimental data to prove this assertion for rotating blades. The primary focus of this work is to demonstrate an arrangement of a passive tubercle based flow control method that can effectively suppress flow separations on the blades and validation of tools and methods that can be used to design and analysing of the next generation of propellers.

1.1 Propeller Geometry

The propeller geometry used in this study derived from that developed for the recent UK MENtOR research project funded by EPSRC. The blades are a generic design based on those typically seen on tilt-rotor aircraft. The propeller has three blades of span 391.2mm.

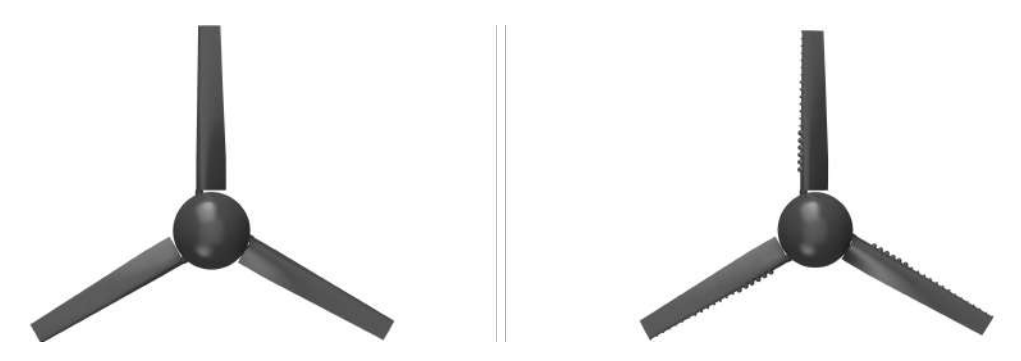


Figure 1 – CAD Geometry for Baseline configuration (left) and Full Tubercle configuration (right)

Span location	$r(\mathbf{mm})$	thickness (mm)	local chord (mm)	twist (deg)	Aerofoil
root	76.18	18.95	60.4	15.89	v43015
Tubercle 1	117.48	16.73	59.2	12.29	v43015
Tubercle 2	132.18	16.03	58.9	10.86	v43015
Tubercle 3	146.48	15.02	57.9	9.6	v43015
Tubercle 4	160.78	13.69	56.8	8.27	v43015
Tubercle 5	175.08	12.42	55.8	7.35	v43015
Tubercle 6	189.48	11.03	54.7	6.01	v43015
Tubercle 7	203.68	9.73	53.7	5.01	v43015
Tubercle 8	217.98	8.43	52.8	4.4	v43015
Tubercle 9	232.28	7.63	51.9	3.87	v43015
Tubercle 10	246.48	7.33	51	2.81	NACA6412
Tubercle 11	260.68	7.03	50.13	2.04	NACA6412
Tubercle 12	275.08	6.71	49.3	1.27	NACA6412
Tubercle 13	289.48	6.4	48.4	0.62	NACA6412
Tubercle 14	303.78	6.09	47.6	0	NACA6412
Tubercle 15	318.08	5.79	46.8	-0.64	NACA6412
Tubercle 16	332.38	5.47	45.9	-1.25	NACA6412
Tubercle 17	346.58	5.17	44.9	-1.79	NACA6412
Tubercle 18	360.78	4.94	44.38	-2.33	NACA6412
Tubercle 19	375.08	4.57	43.5	-2.88	NACA6412
tip	391.18	4.27	43	-3.5	V23010

Table 1 – Tubercles Blade Profile

The geometry was initially drawn in CAD software, with specific propeller dimensions and blade angles, as shown in Figure 1. Table 1 provide the details of the geometry profiles used.

Most of the research conducted relating to tubercles have been for geometries designed as a sinusoidal wave on the leading edge. However by observing Figure 2 (a), it can be seen that tubercles are not exactly sinusoidal waves but rather have peaks extruding outwards at different sizes at irregular intervals along the span of the flippers. It was decided for this project that the tubercles would be designed as a cylindrical extrusions with a hemisphere shape at the end of the cylinder as shown in Figure 2 (b). After the Baseline new CAD geometries were generated in which tubercles were applied at the Leading edge matching the experimental configuration. The size of tubercles was different at the root, middle and tip regions. The diameter of large inboard tubercles was 10.75 mm, the diameter of medium tubercles was 5.73 mm, and the diameter of small tubercles was 3.58 mm. Also, the space between two tubercles was a constant 20 mm, as can be seen in Figure 3.

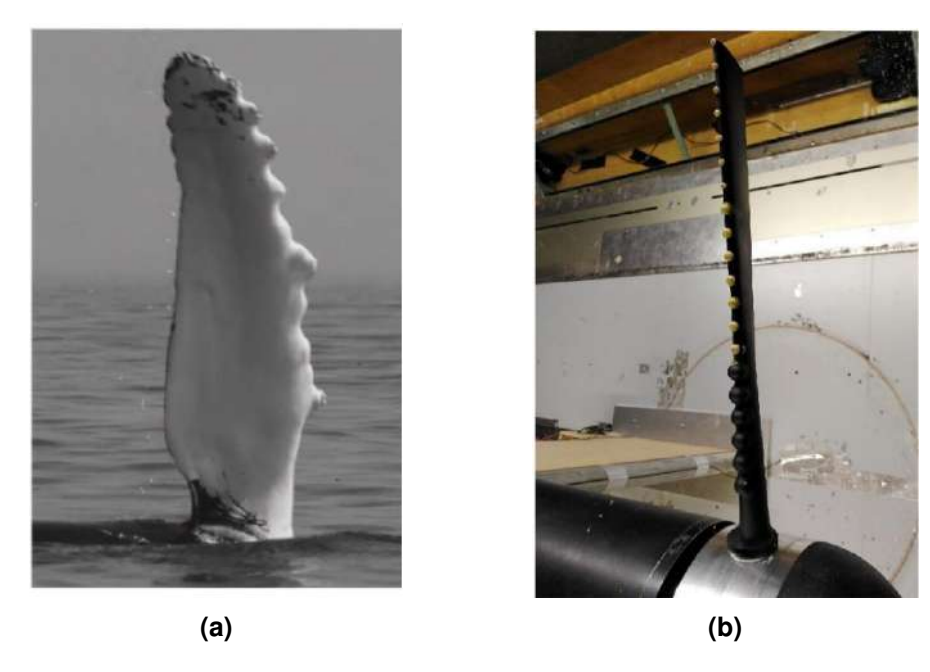


Figure 2 – Bio-mimicry of tubercles from humpback whale flipper used in the leading edge of the propeller blades

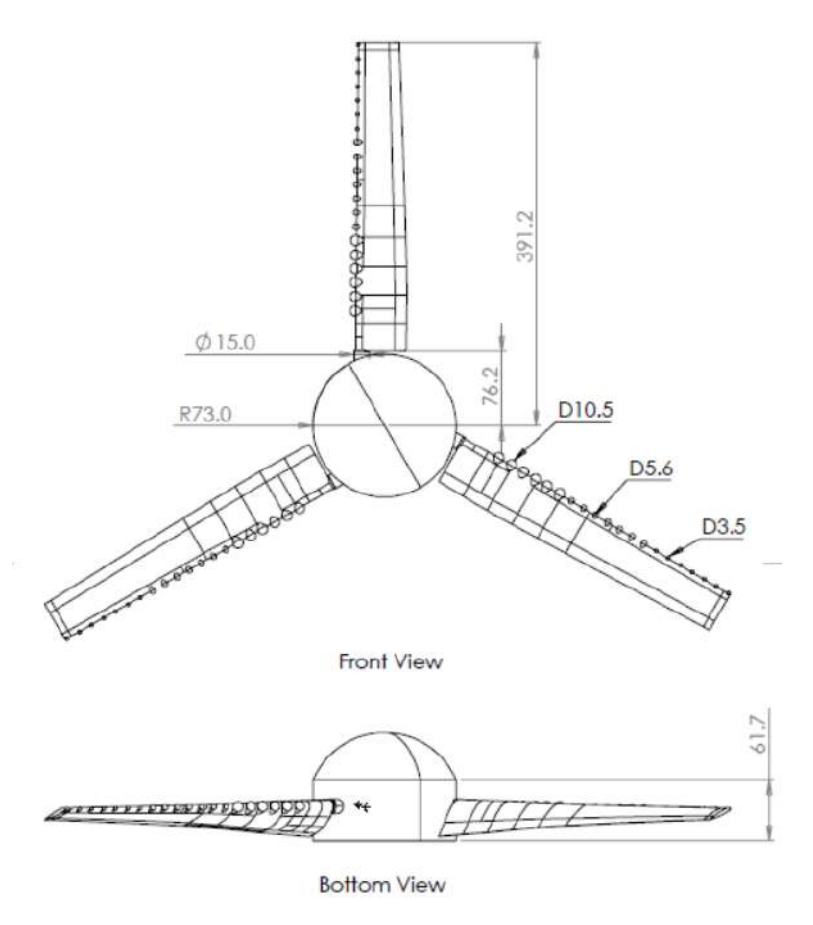


Figure 3 – CAD sketch of propeller geometry with tubercles.

2. Methodology

2.1 Experimental Methodology

A new propeller rig was designed and manufactured at Cranfield for the recent MENtOR project, capable of measuring propeller thrust, vibrational accelerations, rotor speed and power input. The propeller has a swept diameter of 0.782 m. The propeller blades were made of aluminium grade 6082T6 and were manufactured using CNC machining. The three blades were mounted in the hub using a mechanism that allows the blade pitch angle to be smoothly varied and set. Images of the propeller rig and the 8x6 Wind Tunnel test section are displayed in Figure 4.



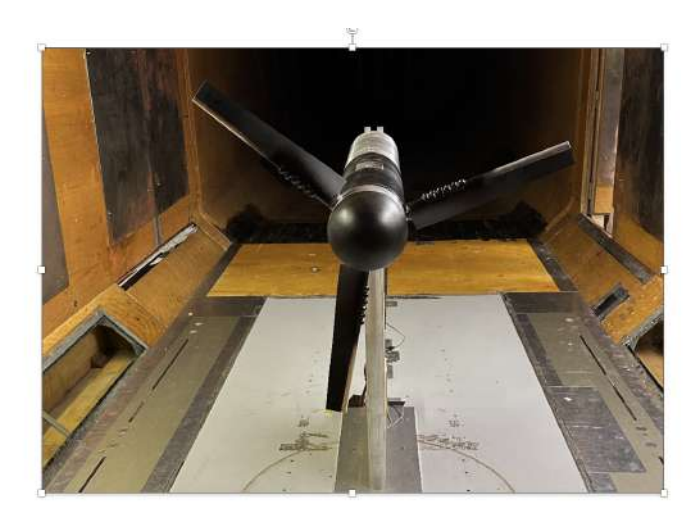


Figure 4 – Propeller test rig in the Cranfield University 8x6 Wind Tunnel.

The propeller shaft is driven by a Dualsky GA 6000 electric motor, which delivers a maximum output of 6.8 kW. A 130 amp electronic speed controller (ESC) was coupled to the electric motor and a watt meter is connected between the ESC and a 2-phase power converter. Two sets of gearboxes can be used in the experiments. To control the angular velocity a Mant is 10A OPTO HV controller was used. The controller has capabilities up to 5000 RPM however the experiment was limited to 3000 RPM due to windmilling and safety concerns. To measure the angular velocity produced, an optical speed sensor, VLS/DA/LSR, was used. Two FC22 compression load cells were employed in the experiment to capture the axial forces, the thrust force being acquired by taking off the measured tare forces from the nacelle. Along each blade at the root there are six screws for large tubercles, seven screws for medium tubercles at the mid-section and seven holes for pins for small tubercles at the tip. The tubercles could be placed and removed from the blade leading edge in order to test different tubercle configurations. Figure 2 (b) show an example where all the tubercles are inserted along the blade, displaying the location and size of the different vortex generators used in the work.

The experimental campaign involved tests in static conditions (wind-off) and also with a wind speed of 10m/s, acquiring data a different RPM for blade pitch angles between negative 2deg to positive 12deg. The blade pitch angle was defined as the angle between the blade tip chord line and the rotational plane. CFD simulations, undertaken before the tests took place, were conducted at three different blade pitch angles (0° , 4.4° and 7.8°), corresponding with previous experimental data, but more numerical calculations are being computed for more blade pitch cases.

2.2 Numerical Methodology

Three different aerodynamic flow solver were employed in the study:

2.2.1 Flow solver - Ansys Fluent

ANSYS Fluent is a widely-used computational fluid dynamics (CFD) software package that numerically solves the conservation equations for fluid flow. At its core are the Navier-Stokes equations, which describe conservation of mass, momentum, and energy in a viscous fluid. For turbulence modeling, Fluent includes Reynolds-Averaged Navier Stokes (RANS) approaches like the k-epsilon,

k-omega, Spalart-Allmaras, and Reynolds Stress transport models. The turbulence modeling selected for this CFD study of is the k-omega model available in ANSYS Fluent. The k-omega model is a two-equation eddy viscosity model that solves transport equations for the turbulence kinetic energy (k) and the specific dissipation rate (ω) , representing the ratio of turbulence energy dissipation rate over k [4]. It is an empirical model that incorporates effects of turbulent velocity gradients and turbulence frequency, useful for analyzing wall-bounded flows and flows with adverse pressure gradients [5]. Compared to other models like k-epsilon, the k-omega formulation can better capture turbulence properties near walls next to no-slip boundaries. For the simulations in this work, the k-omega shear stress transport (SST) variant is selected over the standard version as it includes a blending function to transition from a k-omega formulation in boundary layer regions to a k-epsilon behavior in free shear regions [6]. This aims to improve accuracy across both wall-bounded and free shear/mixing regions within the single computational domain.

2.2.2 Ansys Fluent computational setup

The domain was split into a global stationary domain and a subdivided rotating region. The rotating domain was specified by a smaller cylinder enclosing the blades and the hub. For this rotating domain the enclosure was set 1.2D and 0.5D (with D the diameter of the propeller blade). It is important to note that the rotational domain is cylindrical in shape which allows imparted rotational properties (set by the solver) to be circumferentially equal. The global domain was referred to as the stationary domain because it had zero translational and rotational velocities. A rectangular cuboid enclosure was taken as the flow domain, with the inlet at a distance of 5D from the blade, and the exit at 8D downstream of the same point, as shown in Figure 5. Such sizing ensured that the boundary conditions are sufficiently far from the propeller disc, in order to prevent the full development of the upstream and downstream flow from affecting the results of analysis.

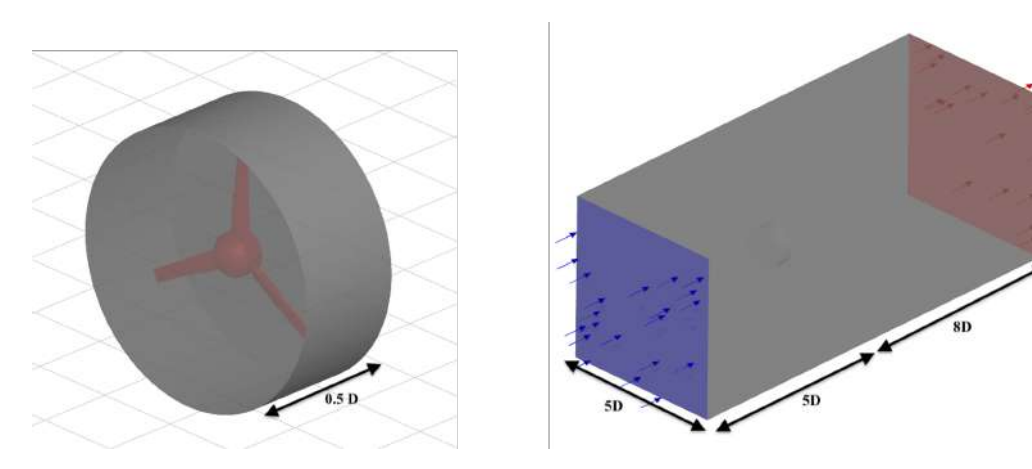


Figure 5 – Computational Domain consisting of a cylindrical rotational domain (left) and a global stationary domain (right).

The computational mesh was generated for the entire flow domain and propeller. The exact pressure distribution and possible separations on the blade are very important for proper thrust computation. Therefore, full boundary layer resolution was desirable. A detailed view of the mesh can be seen in Figure 6. The mesh was hybrid and unstructured, with 20 prism layers around the propeller geometry. The size of the mesh elements was chosen to provide acceptable mesh quality and fully solve the blade's boundary layer, which, in the Fluent solver's case, requires a y+ value below 5 as can be seen in Figure 7.

For the current study, the cell sizes of the mesh were generated to be in a smaller range along the blade in the rotating region and to gradually increase toward the stationary region. Ensuring sufficient grid refinements across the interface enhances the accuracy of the results. The meshes used contain nearly 16 million cells and were chosen after a mesh Independence study based on thrust and torque convergence. A steady state simulation taking advantage of the Multiple Reference Frame (MRF) approach was used in this study. This model allows one to connect a rotating domain

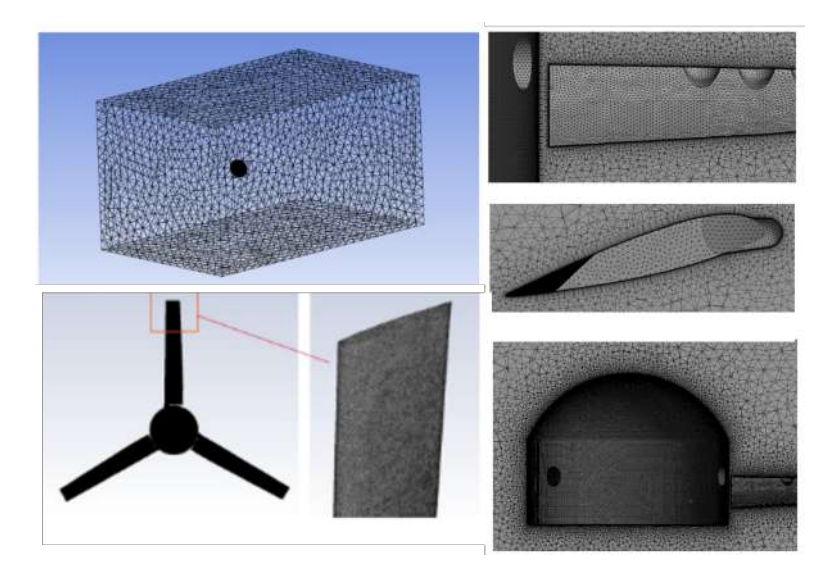


Figure 6 – A detailed view of the Computational Mesh generated by Ansys Meshing.

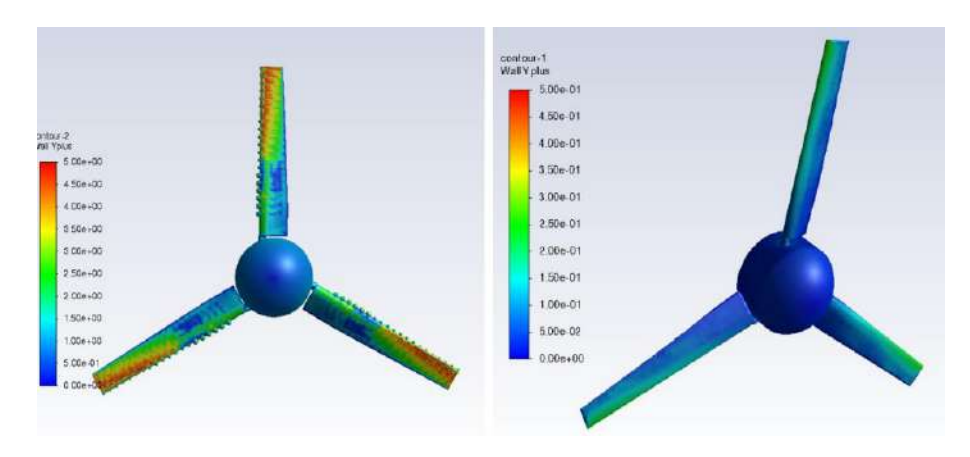


Figure 7 – Wall Y+ values for Full Tubercles and Baseline propeller surface.

containing the propeller blade and its proximity with a complementary stationary domain representing the volume of air further from the propeller. The two domains were connected using domain interfaces of an appropriate type, which transfer data between stationary and rotating frames. In steady state simulation, the domain does not physically move, but only the velocity resulting from domain rotation is added in the appropriate nodes. This leads to a situation where the propeller disc domain is numerically rotating, while the blade remains stationary with respect to the surrounding domain. This method of simulation introduces certain approximation, as the simulation is stationary and the blade itself does not rotate with respect to the surrounding domain. The method is, however, industrially accepted for simulating propellers and provides reliable results.

2.2.3 Flow solver - PowerFLOW

The Lattice Boltzmann Method (LBM) is used to compute the flow field because it was shown to be accurate and efficient for similar low Reynolds number rotor applications [7, 8, 9]. The commercial software 3DS Simulia PowerFLOW has been already validated for aerodynamic and aeroacoustic studies on rotors in general [7, 10, 11]. The software solves the discrete Lattice Boltzmann (LB) equation for a finite number of directions. For a detailed description of the method, the reader can refer to Succi [12] and Shan et al. [13], while to Chen and Doolen [14] for a review. The LB method determines the macroscopic flow variables starting from the mesoscopic kinetic equation, i.e. the LB equation. The discretization used for this particular application consists of 19 discrete velocities in three dimensions (D3Q19), involving a third-order truncation of the Chapman-Enskog expansion [15]. The distribution of particles is solved by means of the LB equation on a Cartesian mesh, known as a lattice. An explicit time integration and a collision model are used. For the collision term, the

formulation based on a unique Galilean invariant [16] is used. The equilibrium distribution of Maxwell-Boltzmann is adopted [15].

To take into account the effect of the sub-grid unresolved scales of turbulence, a Very Large Eddy Simulation (VLES) model is implemented. Following Yakhot and Orszag [17], a two-equations $k-\varepsilon$ Renormalization Group is used to compute a turbulent relaxation time that is added to the viscous relaxation time. To reduce the computational cost, a pressure-gradient-extended wall-model is used to approximate the no-slip boundary condition on solid walls [18, 5]. The model is based on the extension of the generalised law-of-the-wall model [19] to take into account the effect of pressure gradient. These equations are iteratively solved from the first cell close to the wall in order to specify the boundary conditions of the turbulence model. For this purpose, a slip algorithm [14], obtained as generalization of a bounce-back and specular reflection process, is used.

2.2.4 PowerFLOW LBM computational setup

For the LBM setup, a cubic simulation volume of 100D per side is employed, with the propeller geometry positioned at the centre. Boundary conditions are described in Figure 8. The velocity inlet corresponds to the freestream velocity V_{∞} along the Y-axis, while an ambient pressure of 101.325 kPa characterizes the pressure outlet. The blade surface has a no-slip boundary condition.

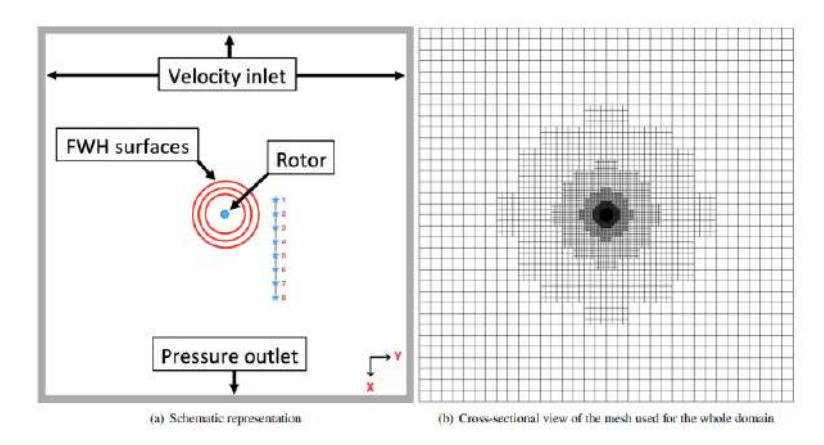


Figure 8 – Simulation domain for the high-fidelity LBM simulation.

The current high-fidelity setup and grid configuration employed in this study are based on the study conducted by Casalino et al. [20]. The previous study extensively tested various grid sizes, and the chosen setup has been adopted as it has demonstrated satisfactory performance. The mesh used for the current propeller setup has been shown in Figure 9 In the finest VR, the values of y+ and voxels per chord are determined to be 30 and 2.7×10^2 , respectively. The y+ value represents a dimensionless parameter indicating the distance of the first cell centre from the computational domain's wall in the wall-normal direction. In the present study, it is computed based on the rotational velocity experienced by the blade at the mid-span location. The voxels per chord parameter, on the other hand, signifies the number of grid cells along the chord direction of the blade and is also evaluated at the blade mid-span location. It is important to note that these grid parameters have been carefully selected and optimized to ensure accurate and efficient simulations in the current investigation, leveraging the knowledge and findings from a previous study on co-rotating propellers [7, 21].

The voxel size corresponding to the finest VR used in the baseline propeller configuration is 0.315 mm. Within the computational domain, the number of fine equivalent voxels is 30.94 million. These fine equivalent voxels are obtained by multiplying the number of voxels by the time stepping rate, which is directly linked to the mesh resolution level. Importantly, doubling the voxel size results in a computational cost reduction of half, as the time step is also doubled accordingly. For the simulations performed in this study, the computational effort is quantified in CPU hours and amounts to 2.01e04 for the simulation of 12 rotor rotations (0.144 s). The simulations were executed on a Linux workstation equipped with an AMD Ryzen Threadripper 3990X Gen3 64 Core 128GB DDR4 3GHz platform. In terms of temporal discretization, the physical time step corresponding to the grid used

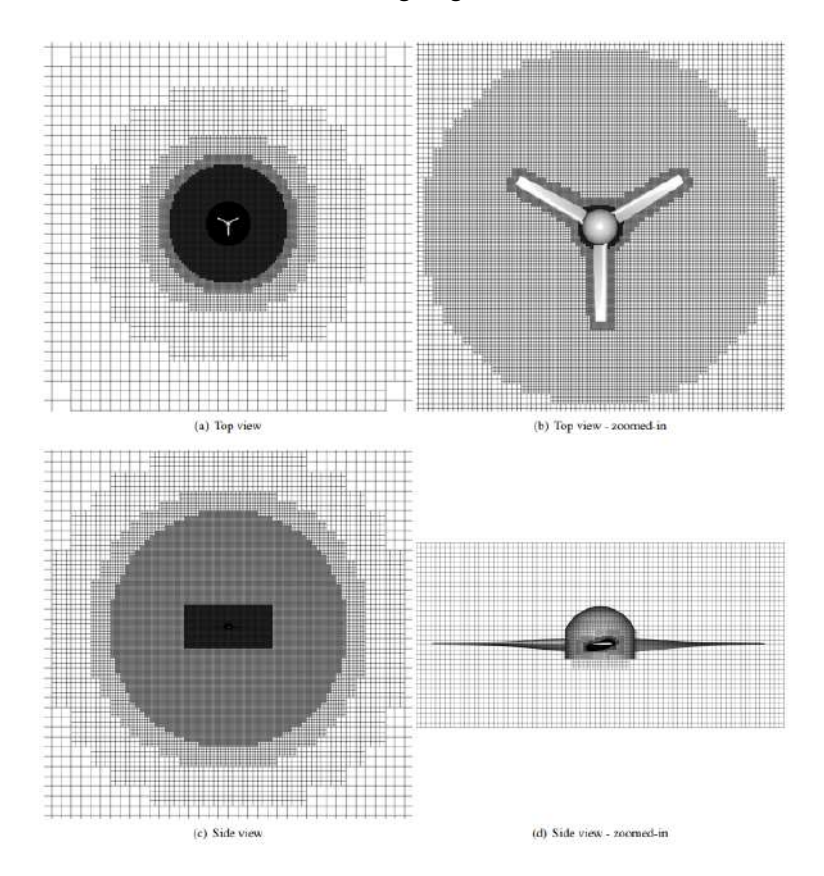


Figure 9 – Cross-sectional view of the mesh for the LBM simulation.

ensures a Courant-Friedrichs-Lewy (CFL) number of 1 in the finest VR level. Consequently, the time step values are determined to be 1.51×10^{-6} s.

2.2.5 Flow solver - FlightStream

FlightStream®, developed by "Research in Flight" since 2014, consists of a reliable, surface vorticity panel code [22] that incorporates viscous boundary-layer corrections. It eliminates the costly process of volume mesh generation and mesh-dependency on flow-field solutions, and stability. It is capable of using structured or unstructured surface meshes and is an intuitive implementation of a classical method for aerodynamic load analysis [23, 24, 25, 26]. FlightStream® uses an unstructured wake-strand model to handle wakes emanating from unstructured meshes [27], as shown in Figure 10.

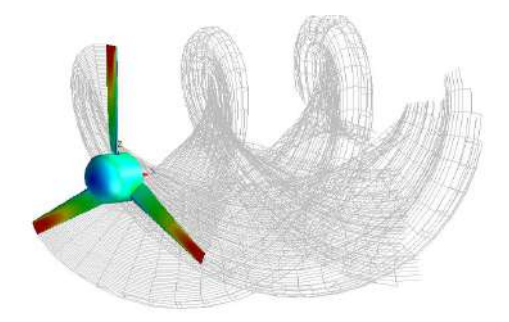


Figure 10 – Example of wakes emanating from the rotating propeller.

The analysis is inviscid, with a separate prediction of the skin-friction drag, separation effects, and high lift influences, based on the surface vorticity. FlightStream® has a model for compressible boundary layers [28] and appropriate separation models derived from classical theory have been implemented with validated fidelity. Collectively, FlightStream® has the fundamental elements required to capture the loads for a very wide variety of subsonic aircraft concepts namely: potential flow theory for the inviscid portions of the flow around the vehicle, comprehensive propeller modeling capabili-

ties using rotating blades and actuator theory, relaxed wakes, propeller wake effects captured [29], skin friction modeling using compressible boundary layer theory, and flow separation modeling to accurately capture lift post stall.

2.2.6 FlightStream computational setup

The distinguishing feature of the surface vorticity-based solver, Flighstream, eliminates the volume meshing process typically required in computational fluid dynamics (CFD) simulations. FlightStream only requires an unstructured surface mesh on the geometry itself. This surface-only meshing approach enhances the efficiency and robustness of the simulations compared to traditional CFD methods relying on volume meshes. The propeller blade surface was discretized using an unstructured mesh with refinements in critical areas as shown in Figure 11. 80 mesh nodes are distributed along the chord to sufficiently resolve the physics in the leading and trailing edge regions, which are key for capturing the boundary layer flow physics. The spanwise direction had 40 nodes. While no 3-dimensional computational domain mesh was needed, other flow parameters like the free stream velocity and operating pressure conditions remain the same as in other computational setups. An unsteady flow solver was set in the computation with a timestep corresponding to 10 degrees of propeller rotation. To model the blade boundary layers effectively, which is critical for resolving viscous effects, viscous coupling and separation modeling features were activated in the solver.



Figure 11 – Flightstream Surface Mesh Grid for BSL configuration: Chordwise 80 nodes and Spanwise 35 nodes.

The number of cells were also increased on the tubercles and region behind the tubercles to capture the chord wise counter-rotating vortices produced by the tubercles as shown in Figure 12.

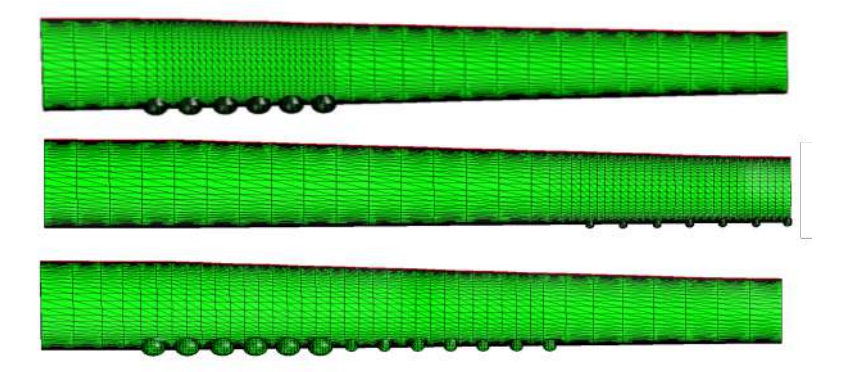


Figure 12 – Flightstream Surface Mesh Grids for tubercles configurations showing the grid refinement in the tubercle regions.

3. Results Discussion

Figures 13 - 15 present the comparisons of the experimentally measured thrust force versus rotor speed for the smooth blade and the full span tubercles configurations for three blade pitch cases. Figure 13 presents the comparison for the zero blade pitch case, and shows that the tubercles begin to progressively increase the thrust for rotor speeds above about 1500 RPM. Detailed experimental flow visualisation needs to be conducted to understand the physics of this effect, but it is expected that the tubercles generate boundary layer embedded vortices that regenerate the boundary layer, particularly inboard where separation is known to occur where local twist angle is very high, and reduce the extent of these separations. Figure 14 presents the corresponding result for a blade pitch angle of 4 degrees where a similar trend is observed, but the relative increase in thrust with tubercles

is less than for the zero blade pitch case. With more extensive inboard separation, it is likely that the tubercles have less authority in suppressing these. Finally figure 15 presents the corresponding result for a blade pitch angle of 8 degrees where the relative improvement with tubercles is further reduced.

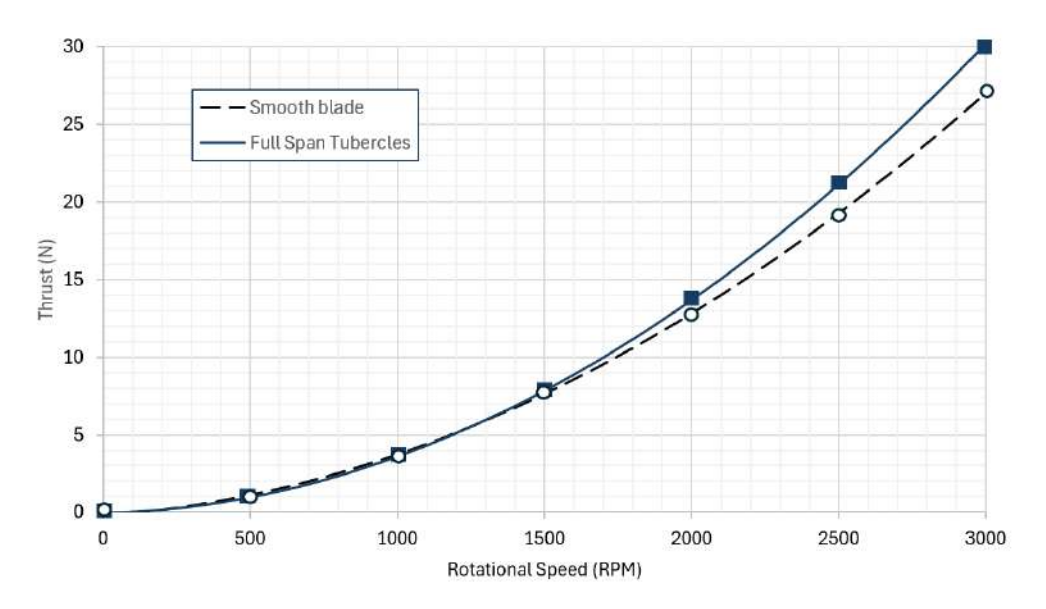


Figure 13 - Thrust versus rotor speed for blade pitch of 0deg

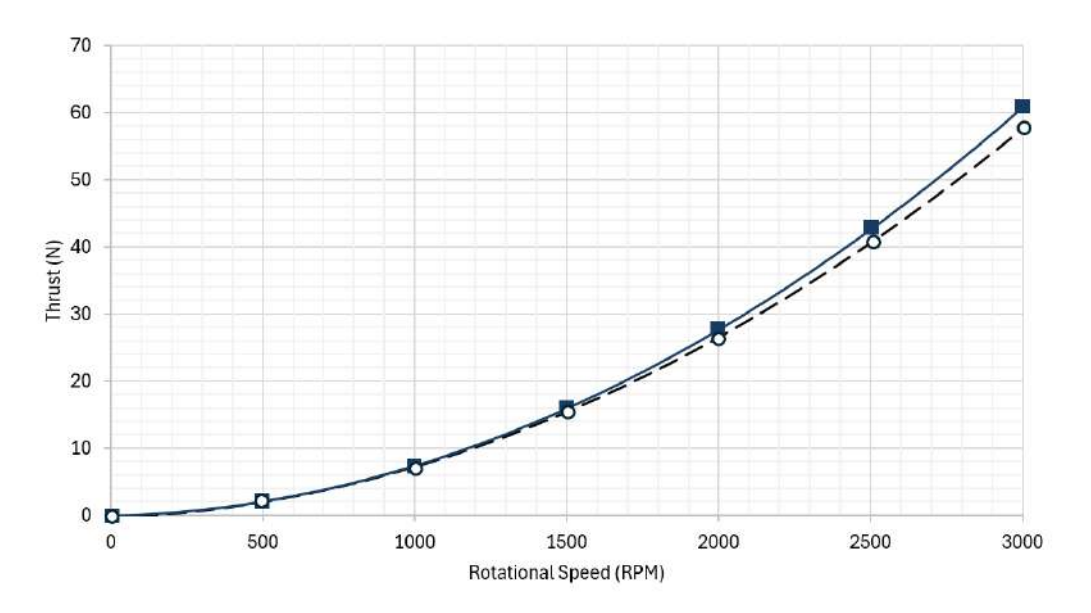


Figure 14 - Thrust versus rotor speed for blade pitch of +4deg

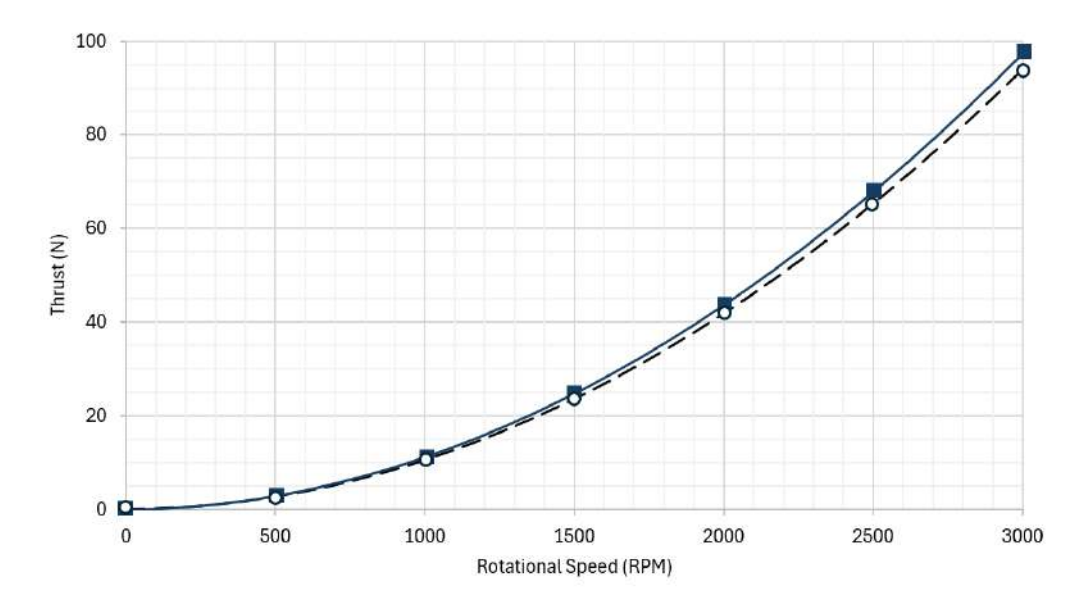


Figure 15 – Thrust versus rotor speed for blade pitch of +8deg

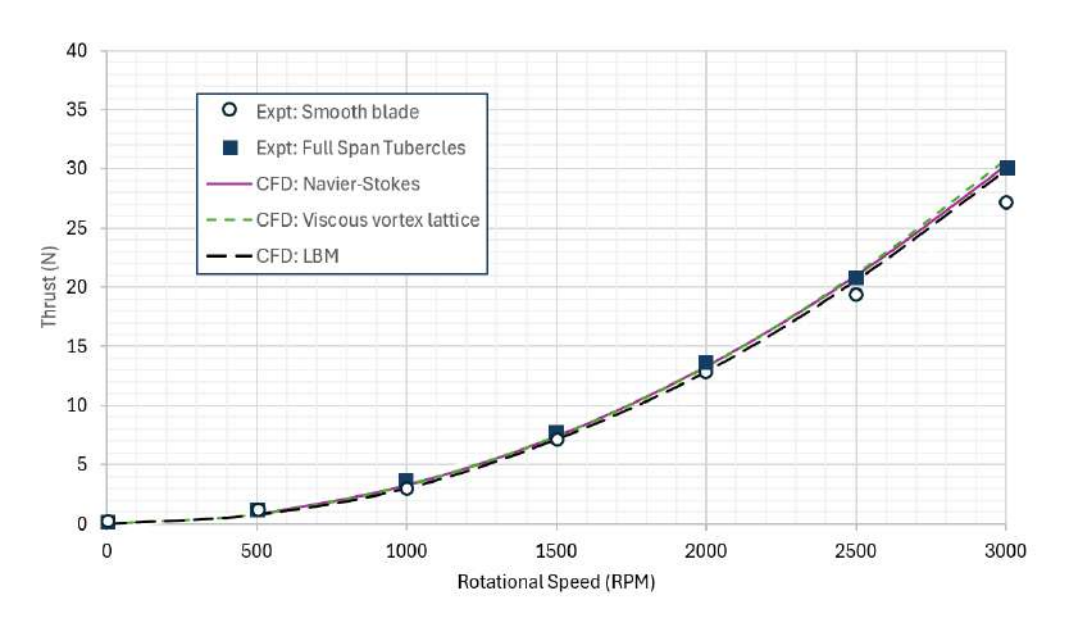


Figure 16 – Variation of thrust generated by the BSL configuration with rotor speed (RPM) as predicted by the three different solvers, compared with experimental data for the zero blade pitch case, with no wind.

On the numerical side, the three flow solvers were run for the baseline smooth configuration (BSL) at $0ms^{-1}$ freestream velocity and 0° blade pitch angle. The results in terms of thrust vs RPM were compared and shown similar results as displayed in Figure 16. Interestingly the numerical predictions, which all agree to a remarkable degree, present a thrust curve that matches, above an RPM of 2000, the full span tubercle experimental result, rather than that measured for the baseline smooth case. This suggests that the experimental flow might have been more transitional in nature, than fully turbulent, and this is something that needs further investigation.

The described RANS CFD numerical model was used to simulate the propellers at six different rotational speeds, from 500 to 3000, with an increment of 500 RPM, with a zero freestream velocity. In order check the correct simulation set up, the blade velocity vector in the standard frame and the 3D streamline coming towards the propeller have been visualised and reported for the baseline case rotating at 3000RPM, as shown in Figure 17 Specifically, two configurations have been tested so far, with tubercles applied just outboard (small) and applied all over the leading edge span (large, medium and small - LMS configuration), as in Figure 18, in addition to the baseline propeller geometry (no

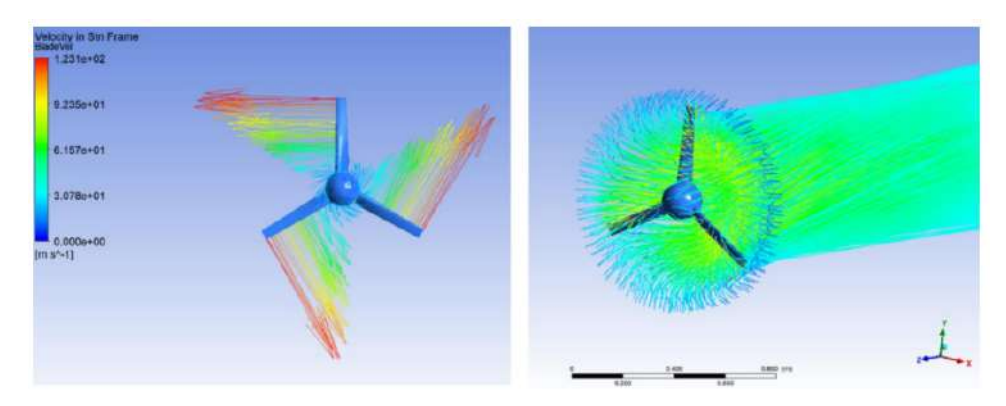


Figure 17 – Velocity vectors (left) and 3D streamlines (right) for the Baseline propeller case.

tubercles).

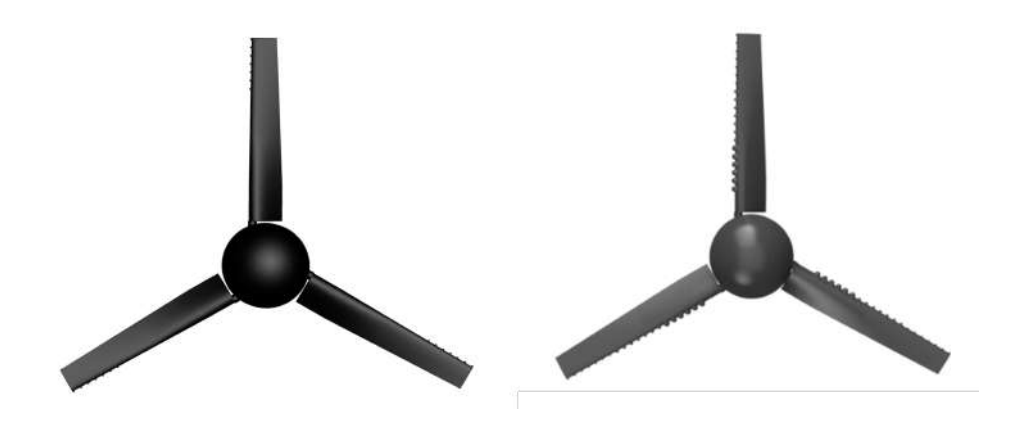


Figure 18 – CAD of Propeller with Tubercles at leading edge tested. Small tubercles configuration (left) and full tubercles configuration (right)

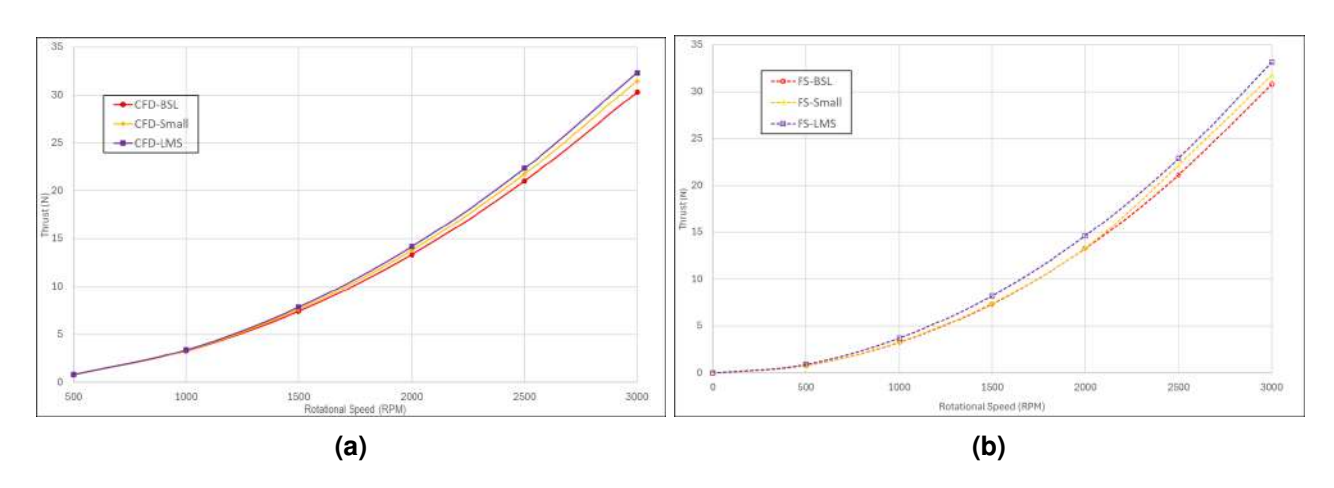


Figure 19 – Comparison of thrust variation with angular velocity for LMS and small tubercle configuration with BSL, using two different Aerodynamics solver.

Figure 19 reports the thrust produced by both the tubercles configurations in comparison with BSL configuration, using both Fluent and FlighStream for blade pitch angle set to zero. FlightStream slightly predict a slightly higher thrust values than Fluent for the two tubercles configurations, but the their trend is the same. The baseline model and the tubercles configuration have nearly similar thrust values at lower rotational speed, but as the rotational speed increases the gain in term of performance is more pronounced, and this is more evident for the case when tubercles are applied along the entire leading edge 19(a), with an average thrust improvement of 8%. For the other case analysed, tubercles applied just outboard (Small), the thrust improvement is less conspicuous 19(b),

with an average improvement of 4% compared to the baseline (BSL) configuration. As for the different pitch angles numerically studied, 4.4 and 7.8 degrees the results once again have the same trend observed during the experiments, which is a decrease in thrust gain increasing the blade pitch angle, as shown in Figures 20 and 21.

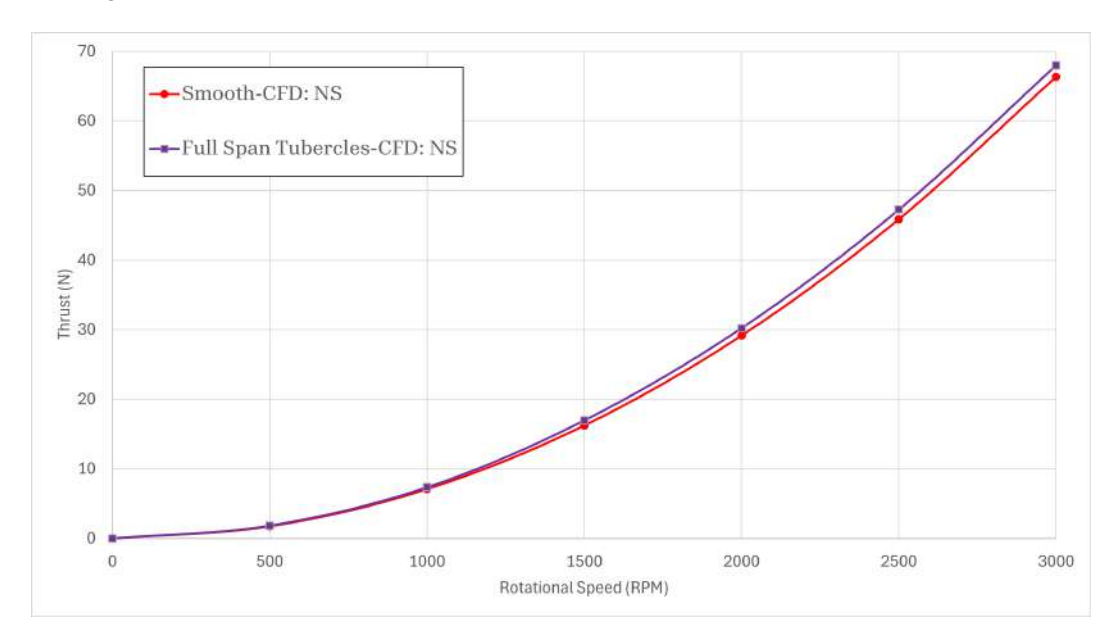


Figure 20 - Thrust versus rotor speed for blade pitch of +4.4deg

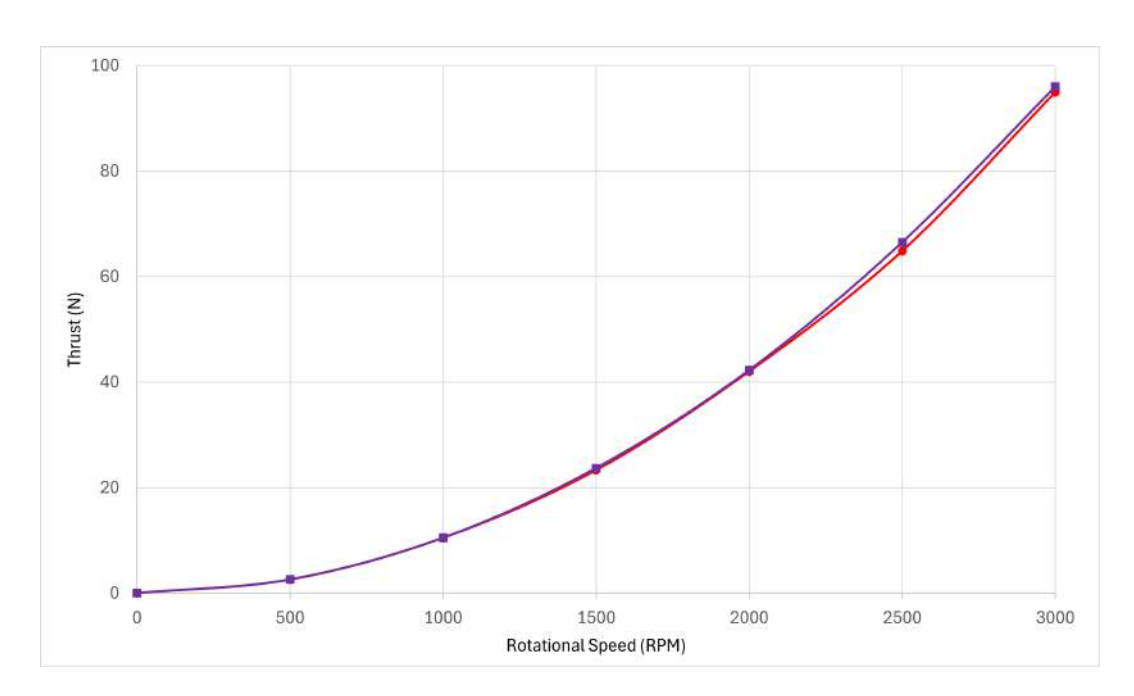


Figure 21 – Thrust versus rotor speed for blade pitch of +7.8deg

The effects on how the tubercles affects the flow physics is shown in term of static pressure and skin friction coefficient respectively in Figures 22 and 23 for a case with no wind and at a rotational speed of 3000 RPM. It is possible notice a better pressure recovery close to the trailing edge for the tubercles configuration compared to the baseline blade from the static pressure contour and a delay in flow separation from the skin friction contour particularly in the inner part of the blades.

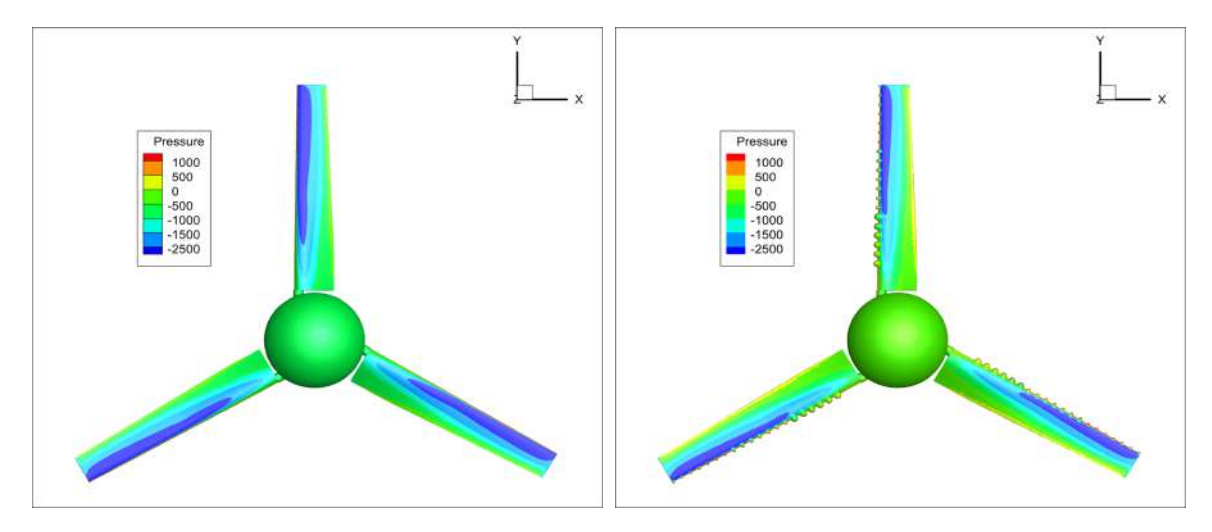


Figure 22 – Static pressure contour comparison: BSL (left), Full span tubercles (right)

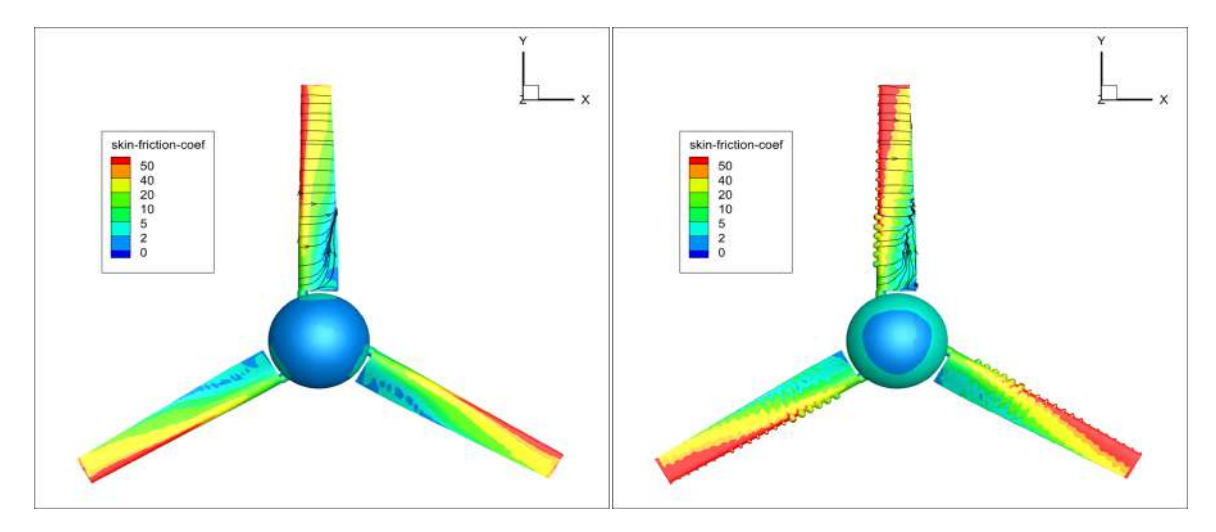


Figure 23 – Skin Friction contour comparison: BSL (left), Full span tubercles (right)

4. Conclusion

A parametric study was undertaken to investigate the effects of leading-edge tubercles on the performance of a three-bladed reference propeller utilizing the three different CFD solvers - Fluent, Lattice Boltzmann Method (PowerFlow), and Surface Vorticity Based solver (FlightStream). The location of the tubercles along the blade span was varied across different propeller configurations. These simulations were performed over various rotational speeds. Reynolds-averaged Navier-Stokes (RANS CFD) Vorticity Based solver and results for the small and LMS tubercle configurations at zero wind speed and blade pitch angle have indicated 4% and 8% average thrust improvements compared to the baseline propeller. The numerical results were validated against wind tunnel experimental data and the agreement was found to be good, and more importantly the trend was properly captured. A more systematic parametric study will be undertaken to analyse more propeller configurations in term of the location of the tubercles along the blade span under different wind speeds. Further CFD simulations of other tubercle configurations and experimental testing in the Cranfield University 8x6 Wind Tunnel are planned in the coming months. Following post-processing, the relationships between thrust,

torque, and tubercle parameters will be characterized, along with variations in performance attributed to modifications of the blade-surface flow mechanisms due to the tubercles. From this investigation was found that the Navier-stokes simulation needs about 30 hrs for a converged solution using 64 CPUs in a HPC system, the LMB code took an average of 9 hours and the unsteady vorticity panel solver around 5 hours for any of the RPMs simulated both using a standard workstation for a total of eight blade rotations. The three computational approaches will also be further compared regarding solution accuracy and computational expense when more wind tunnel experiments will be available to ascertain the most suitable methodology for modelling this class of problem.

5. Contact Author Email Address

mailto: davide.dipasquale@cranfield.ac.uk

6. Copyright Statement

The authors confirm that they, and/or their company or organization, hold copyright on all of the original material included in this paper. The authors also confirm that they have obtained permission, from the copyright holder of any third party material included in this paper, to publish it as part of their paper. The authors confirm that they give permission, or have obtained permission from the copyright holder of this paper, for the publication and distribution of this paper as part of the ICAS proceedings or as individual off-prints from the proceedings.

References

- [1] H. Johari, C. Henoch, D. Custodio, and A. Levshin. Effects of leading-edge protuberances on airfoil performance. https://doi.org/10.2514/1.28497, 45:2634–2642, 5 2012.
- [2] Zhaoyu Wei, T. H. New, and Y. D. Cui. An experimental study on flow separation control of hydrofoils with leading-edge tubercles at low reynolds number. *Ocean Engineering*, 108:336–349, 11 2015.
- [3] D. Custodio, C. W. Henoch, and H. Johari. Aerodynamic characteristics of finite span wings with leading-edge protuberances. *AIAA Journal*, 53:1878–1893, 2015.
- [4] ANSYS INC. Ansys fluent theory guide. 2022.
- [5] D C Wilcox. Turbulence modelling for CFD (Third Edition). DCW Industries, Incorporated, 2006.
- [6] F R Menter. Two-equation eddy-viscosity turbulence models for engineering applications. *AIAA Journal*, 1994.
- [7] Shubham Shubham, Francesco Avallone, Edoardo Grande, and Damiano Casalino. Computational aeroacoustic investigation of co-rotating rotors for urban air mobility. 12 2021.
- [8] Shubham Shubham, Nigel Wright, and Anton Ianakiev. Application of richardson extrapolation method to aerodynamic and aeroacoustic characteristics of low reynolds number vertical axis wind turbines. page 3022, 2022.
- [9] Nicolas Gourdain, Thierry Jardin, Ronan Serre, Sebastien Prothin, and Jean-Marc Moschetta. Application of a lattice boltzmann method to some challenges related to micro-air vehicles. *International Journal of Micro Air Vehicles*, 10:285–299, 2018.
- [10] Damiano Casalino, Andreas Hazir, and Adrien Mann. Turbofan broadband noise prediction using the lattice boltzmann method. *AIAA Journal*, 56:609–628, 2018.
- [11] Clement Nardari, Damiano Casalino, Francesco Polidoro, Vedran Coralic, Phoi-Tack Lew, and John Brodie. Numerical and experimental investigation of flow confinement effects on uav rotor noise. page 2497, 2019.
- [12] S Succi. *The lattice Boltzmann equation for fluid dynamics and beyond.* Clarendon Press, 1st editio edition, 2001.
- [13] Xiaowen Shan, Xue Feng Yuan, and Hudong Chen. Kinetic theory representation of hydrodynamics: A way beyond the navier-stokes equation. *Journal of Fluid Mechanics*, 550:413–441, 2006.
- [14] Shiyi Chen and Gary D Doolen. Lattice boltzmann method for fluid flows. *Annual Review of Fluid Mechanics*, 30:329–364, 1998.
- [15] Hudong Chen, Shiyi Chen, and William H Matthaeus. Recovery of the navier-stokes equations using a lattice-gas boltzmann method. *Physical Review A*, 45, 1992.
- [16] H Chen, R Zhang, and P Gopalakrishnan. Lattice boltzmann collision operators enforcing isotropy and galilean invariance, 12 2015.
- [17] Victor Yakhot and Steven A Orszag. Renormalization group analysis of turbulence. i. basic theory. *Journal of Scientific Computing*, 1:3–51, 12 1986.

Effects of Leading Edge Tubercles on the Performance of Rotating Propeller

- [18] C M Teixeira. Incorporating turbulence models into the lattice-boltzmann method. *International Journal of Modern Physics C*, 09:1159–1175, 12 1998.
- [19] B E Launder and D B Spalding. The numerical computation of turbulent flows. *Computer Methods in Applied Mechanics and Engineering*, 3:269–289, 1974.
- [20] Damiano Casalino, Edoardo Grande, Gianluca Romani, Daniele Ragni, and Francesco Avallone. Definition of a benchmark for low reynolds number propeller aeroacoustics. *Aerospace Science and Technology*, 113:106707, 2021.
- [21] Shubham Shubham. Computational aeroacoustic investigation of co-rotating rotors for urban air mobility. 2020.
- [22] Vivek Ahuja and R J Hartfield. Aerodynamic loads over arbitrary bodies by method of integrated circulation. https://doi.org/10.2514/1.C033619, 53:1719–1730, 12 2016.
- [23] By L Prandtl. Applications of modern hydrodynamics to aeronautics. 1925.
- [24] A Plotkin International Journal of Aerodynamics and undefined 2012. Low-speed aerodynamics the theoretical aspects. *inderscienceonline.com*, 2:1, 2012.
- [25] J T Conway Journal of Fluid Mechanics and undefined 1995. Analytical solutions for the actuator disk with variable radial distribution of load. *cambridge.orgJT ConwayJournal of Fluid Mechanics*, 1995•cambridge.org.
- [26] Daniel J Strash, David A Lednicer, and Theodor D Rubin. Analysis of propeller-induced aerodynamic effects. *16th AIAA Applied Aerodynamics Conference*, pages 96–104, 1998.
- [27] Erik D Olson and Cindy W Albertson. Aircraft high-lift aerodynamic analysis using a surface-vorticity solver. 54th AIAA Aerospace Sciences Meeting, 0, 2016.
- [28] Hartfield R. J Johnson, S. Full scale investigation of the static longitudinal and lateral characteristics of a light single-engine airplane using a surface vorticity solver and cfd. 2018.
- [29] Vivek Ahuja and Roy J Hartfield. Predicting the aero loads behind a propeller in the presence of a wing using flightstream[™]. *15th AIAA Aviation Technology, Integration, and Operations Conference*, 2015.